THE JOURNAL OF PHYSICAL CHEMISTRY C

Article

pubs.acs.org/JPCC

Nanoconfined $LiBH_4$ and Enhanced Mobility of Li^+ and BH_4^- Studied by Solid-State NMR

Margriet H. W. Verkuijlen,[†] Peter Ngene,[‡] Daan W. de Kort,[†] Charlotte Barré,[‡] Angeloclaudio Nale,[‡] Ernst R. H. van Eck,[†] P. Jan M. van Bentum,[†] Petra E. de Jongh,[‡] and Arno P. M. Kentgens*[,†]

[†]Institute for Molecules and Materials, Radboud University, Heyendaalseweg 135, 6525 AJ Nijmegen, The Netherlands

[‡]Inorganic Chemistry and Catalysis, Debye Institute for Nanomaterials Science, Utrecht University, Universiteitsweg 99, 3584 CG, Utrecht, The Netherlands

Supporting Information

ABSTRACT: The structural and dynamical properties of $LiBH_4$ confined in porous carbon and ordered porous silica are studied using ^1H, ^7Li, and ^{11}B solid-state NMR. The ^{11}B and ^7Li NMR resonances of $LiBH_4$ confined in porous carbon (broad pore size distribution up to <60 nm) are strongly broadened compared to bulk $LiBH_4$. This line broadening is dominated by anisotropic susceptibility effects induced by the nanostructured carbon host. Because of the lack of resolution caused by the anisotropic susceptibility broadening, we studied confined $LiBH_4$ in ordered porous silica (MCM-41 pore size: 1.9 nm). In the ^7Li and ^{11}B spectra, a bulk-like $LiBH_4$ resonance is observed together with an additional, more narrow component. Above T = 313 K, this component showed a typical J-coupling pattern in both ^{11}B and ^1H spectra corresponding to highly mobile BH_4^- species. Static ^{11}B solid-state NMR measurements compared with second moment calculations show that these BH_4^- species not only rotate as in the bulk material but also experience translations through the crystal lattice. Static ^7Li measurements show that Li^+ is also highly mobile. Therefore, we conclude that nanoconfinement of $LiBH_4$ strongly enhances diffusional mobility of borohydride anions and lithium in this material.

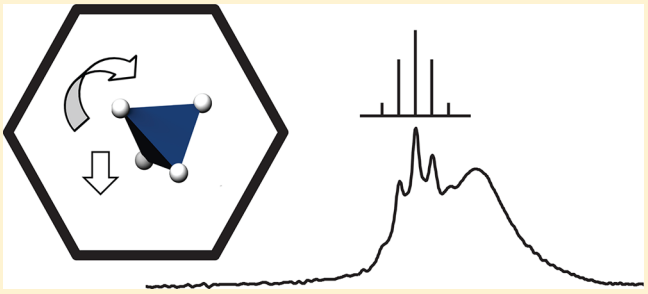

INTRODUCTION

Metal hydrides are promising materials to compactly store hydrogen.[1] The complex metal hydride lithium borohydride, $LiBH_4$, is an interesting material because of its relatively high gravimetric hydrogen content of 18.5 wt % and volumetric hydrogen content of 121 kg H_2/m^3.[2] $LiBH_4$ forms an ionic crystal which contains Li^+ cations and BH_4^- anions. Motion is present throughout the lithium borohydride crystal. Several studies on atomic mobility in the $LiBH_4$ crystal lattice report rapid reorientations of the tetrahedral BH_4^- anions.[2−7] The material melts at 558 K and undergoes a solid−solid phase transition from a low-temperature orthorhombic phase to a high-temperature hexagonal phase at 384 K.[8] The high-temperature phase shows a remarkable higher Li ion mobility than the low-temperature phase.[9]

In practical applications, $LiBH_4$ is unfortunately thermodynamically too stable, and high temperatures are needed to release its hydrogen. The overall decomposition reaction, when the material is heated up to 773 K, is shown to be according to the scheme[2]

$$LiBH_4(l) \rightarrow LiH(s) + B(s) + 3/2H_2(g) \quad (1)$$

where $Li_2B_{12}H_{12}$ generally has been accepted as a intermediate species.[10−12] The decomposition of LiH is usually not taken into account since LiH is stable up to 1173 K.[13] Another issue in practical applications of $LiBH_4$ is that the hydrogen desorption reactions are not fully reversible. Partial reversibility has been shown at a hydrogen pressure of 155 bar and a temperature of 873 K.[14]

One of the methods to improve hydrogen sorption kinetics and reversibility in metal hydrides is by confinement in a nanoporous support material, which results in a reduction of the particle sizes to the nanoscale.[15−21] The kinetics of the reactions of the desorption and absorption of hydrogen are significantly improved, and the thermodynamics properties have been shown to be modified for $NaAlH_4$.[22,23] For $LiBH_4$, Gross et al.[24] reported for the first time enhanced kinetics after nanoconfinement by melt infiltration in a porous carbon aerogel.

To study structure and dynamics of (complex) metal hydrides, solid-state NMR has become a popular technique.[5,6,25−32] Hwang et al.[11] confirmed the formation of $B_{12}H_{12}^{2-}$ complexes in the decomposition of metal borohydrides by NMR. Conradi et al.,[4,6,32,33] Skripov et al.,[5,7] and

Received: June 22, 2012
Revised: September 24, 2012
Published: September 25, 2012

Jimura et al.[34] studied the structure and atomic mobilities of $LiBH_4$.

Jimura et al.[34] showed, using solid-state NMR, that two types of motion take place for a BH_4^- unit in the low-temperature phase. The second moments of the ^1H and ^{11}B spectra suggest that the sum of these two types of motion resembles isotropic reorientation of the BH_4^- unit. This motion is observed for $T >$ 170 K, and the rotation rates exceed a threshold value in the order of in the kHz range. In addition, the rotational motion of BH_4^- in $LiBH_4$ has recently been studied by quasielastic and inelastic neutron scattering, which can probe H motions that occur on the order of nanoseconds to picoseconds. The results of Verdal et al.[35] strongly suggest a reorientation mechanism for BH_4^- in the high-temperature phase (above 384 K) of $LiBH_4$ described by a trigonal-axis rotation of three borohydride H atoms coupled with jump exchanges with the remaining axial H atom.

Martelli et al.[36] report that the motion of BH_4^- in $LiBH_4$/LiI solid solutions is dominated by 90° reorientations around the 4-fold symmetry axes of BH_4^-. At temperatures about 200 K, typical dwell times between these reorientational jumps are in the picosecond range. The presence of iodide enhances the reorientation speed and stabilizes the disordered high-temperature phase of $LiBH_4$ well below room temperature.

For nanoconfined complex metal hydrides, NMR is particularly valuable,[32,37−42] since the outcome of solid-state NMR experiments is mainly influenced by the local structure and no long-range crystallinity is required. For example, X-ray invisible phases of nanoconfined $LiBH_4$ formed after melt infiltration and rehydrogenation could be identified by solid-state NMR.[41] In this work, we will describe the effect of confinement in porous carbon and ordered porous silica on the structure and dynamics of $LiBH_4$ by ^1H, ^7Li, and ^{11}B solid-state NMR.

EXPERIMENTAL SECTION

Synthesis of the Samples. High surface area graphite (HSAG-500, Timcal Switzerland) and ordered porous silica MCM-41 (synthesis described below) were used as nanoporous materials to confine $LiBH_4$ (Acros Organics, 95% pure). All sample handling and storage was done under an Ar atmosphere in a glovebox (contamination typically less than 0.1 ppm of O_2 and H_2O) to avoid exposure to O_2/H_2O.

MCM-41 was synthesized according to a procedure described by Cheng et al.[43] using cetyltrimethylammonium bromide (CTAB, Aldrich) as template, Aerosil 380 (Evonik) as silica source, and tetramethylammonium hydroxide (TMAOH, 25% Aldrich) as base. 6.28 g of CTAB was dissolved in a solution containing 55.37 g of water and 6.07 g of TMAOH. Then 5 g of Aerosil 380 was added, and the solution was stirred for 1 h at 313 K to form a gel. The gel was aged in a Teflon-lined autoclave at 353 K for 24 h and subsequently crystallized at 413 K for 48 h. The resulting product was filtered and washed extensively with water until pH was neutral, dried at 333 K for 24 h, and calcined at 723 K for 10 h.

The porosity was characterized using nitrogen physisorption, and the pore size distributions of the samples were calculated from the adsorption branch using BJH theory[44] with the Harkins and Jura thickness equation (silica−alumina reference for MCM-41) and Carbon Black STSA thickness equation (for HSAG-500). MCM-41 has a narrow pore size distribution centered at 1.9 nm, a single point adsorption total pore volume of 0.66 $cm^3\ g^{-1}$, and a BET surface area of 1550 $m^2\ g^{-1}$. The high surface area graphite has a BET surface area of 500 $m^2\ g^{-1}$ and a single point adsorption total pore volume of 0.68 $cm^3\ g^{-1}$ with 0.5 $cm^3\ g^{-1}$ in pores smaller than 200 nm, of which 50% comes from pores with a diameter smaller than 14 nm. Prior to use, the carbon was dried at 500 °C for 5 h under a N_2 flow.

Host materials were melt infiltrated with $LiBH_4$; the required amounts of carbon and $LiBH_4$ were mixed, placed in a graphite sample holder, and inserted into a stainless steel autoclave. An initial pressure of 50 bar of H_2 was applied. The sample was heated at 3 K min^{-1} to 568 K and allowed to stay for 30 min at 568 K at a final pressure of 100 bar of H_2. The sample was then allowed to cool down to room temperature, and the hydrogen gas pressure was released. $LiBH_4$/C nanocomposites containing 5, 15, 25, 35, 45, and 65 wt % $LiBH_4$ were synthesized and labeled according to the weight percentage of $LiBH_4$ relative to the total weight of the sample. A $LiBH_4$/MCM-41 nanocomposite containing 30 wt % $LiBH_4$ was synthesized by the same procedure used to melt infiltrate carbon.

Considering the pore volume in HSAG-500 and the bulk density of $LiBH_4$ (0.666 g cm^{-3}), 25 wt % sample is expected to fill all pores up to 200 nm, while the 35 wt % sample is expected to be overfilled. Sometimes even at nominal pore filling a small residual pore volume in the range of 4−20 nm is detected, indicating incomplete pore filling. Similarly for the MCM-41, about 30 wt % $LiBH_4$ is required to completely fill all the pores.

As a reference sample, pure $LiBH_4$ without nanoporous material was treated in a similar way as the melt infiltrated samples by heating it under a hydrogen pressure.

Solid-State NMR Measurements. Solid-state NMR experiments were performed on 600 MHz (14.1 T) and 850 MHz (20 T) Varian VNMRS spectrometers using 2.5 mm HX MAS and 1.6 mm HXY MAS probes. All experiments were performed in a flowing dry N_2 environment because of the O_2/H_2O reactivity of the samples.

On the 600 MHz spectrometer, ^{11}B and ^7Li single pulse excitation spectra were obtained using a short hard pulse of 0.20 μs at an effective RF field strength of 140 kHz. A MAS speed of 10 kHz was applied.

Z-filtered ^{11}B MQMAS experiments[45−47] were performed on the 600 MHz spectrometer using high power pulses at an RF field strength of 160 kHz and low power pulses at an RF field strength of 15 kHz and sample spinning speed of 15 kHz. After the 2D Fourier transform, a shearing transformation was applied using a shearing factor equal to 7/9 for ^{11}B (I = 3/2). Different conventions are reported in the literature for the scaling of the F_1 dimension.[48] We multiplied the vertical axes (F_1) of the MQMAS spectrum by a factor of 9/34 for ^{11}B, resulting in equal chemical shift values in ppm in the F_1 and F_2 dimension for a hypothetical resonance without a quadrupolar interaction.[49]

On the 850 MHz spectrometer, ^{11}B and ^7Li single pulse excitation spectra were obtained using a short hard pulse of 0.20 μs at an effective RF field strength of 150 kHz. Continuous wave ^1H decoupling at an RF field strength of 7 kHz was applied after optimization of this field strength. A MAS speed of 17.5 kHz was applied. ^1H single pulse excitation spectra were measured using a 90° pulse at an RF field strength of 150 kHz.

A ^{11}B 2D J-resolved NMR experiment was performed on the 850 MHz spectrometer.[50] A 90° pulse of 1.7 μs and a 180° pulse of 3.4 μs were used at an RF field strength of 160 kHz. Continuous wave ^1H decoupling with a RF field strength of 7 kHz was applied during detection. A MAS speed of 17.5 kHz was applied.

Static ^{11}B and ^{7}Li NMR measurements (without magic angle spinning) were performed using a 1.6 mm HXY MAS probe in a flow of dry nitrogen. The ^{11}B measurements were done on the 850 MHz spectrometer, using a solid echo pulse sequence with τ_{SE} = 50 μs, an RF field strength of 160 kHz, and a 90° pulse length of 1.7 μs. For ^{7}Li, experiments were conducted on the 600 MHz spectrometer, and a short hard pulse of 0.20 μs at an effective RF field strength of 150 kHz was used.

Second Moment Calculations. To calculate the size of the dipolar line broadenings of ^{7}Li and ^{11}B with ^{1}H, ^{6}Li, ^{7}Li, ^{10}B, and ^{11}B nuclei in close proximity, second moment calculations were performed. From the physical point of view, the second moment can be seen as the square of the average local magnetic field induced by the surrounding dipoles at the position of the resonant nucleus. It can be calculated using a set of equations derived from first principles by Van Vleck.[51] In these calculations, the contributions of the different isotopes are weighted by their natural abundances. The calculated second moment dipolar line width is a good prediction for the experimentally determined line width if the crystal lattice is rigid. In NMR, a rigid lattice implies that there are no atomic motions present during the measurement, in particular when the free induction decay is being recorded. If the motion is fast, internuclear distances and angles will vary during the measurement and averaging of the dipolar couplings will take place, leading to a narrowing of the resonances. This effect can be calculated by averaging the second moment for different positions of an atom during the measurement.

In this study of $LiBH_4$, the second moment calculations were performed for a rigid crystal lattice and for this lattice allowing for rotational motion of the BH_4^- anions. The atomic positions, which were determined by synchrotron single-crystal diffraction data, were taken from Filinchuk et al.[52] From the $LiBH_4$ crystal parameters, a 3 × 3 × 3 unit cell array was created, corresponding to a crystal size of 21 × 13 × 10 Å and a total of 108 BH_4^- anions. Including more unit cells in the calculation did not yield a significantly different outcome because of the r^{-6} dependency of the magnetic dipole contribution to the second moment.

The rotation of the borohydride anions was implemented by an iterative model[53−56] in Matlab.[57] An "isotropic" rotation for the BH_4^- was implemented by rotations around the four C_3 symmetry axes of a BH_4^- anion. In every iteration, one of the BH_4^- anions was randomly selected. Then, one of the four C_3 rotation axes was randomly selected, about which a BH_4^- reorientational jump took place either clockwise or counterclockwise. This model of fast isotropically rotating BH_4^- anions will be representative for any reorientation mechanism where the four hydrogen atoms move fast over all four possible positions in the BH_4^- anion. Handling the $^{11}B-^{11}B$ and $^{7}Li-^{7}Li$ terms as like (equal gyromagnetic ratio and orientation/magnitude of the electric field gradient) or semilike (equal gyromagnetic ratio but a different orientation/magnitude of the electric field gradient) spins leads to only slight differences in the overall calculated full width at half-maximum (fwhm).[58] For $LiBH_4$ not all electric field gradient tensors were expected to have the same orientation within a unit cell, and therefore the $^{11}B-^{11}B$ and $^{7}Li-^{7}Li$ terms were approximated by treating them as semilike spin terms.

RESULTS AND DISCUSSION

$LiBH_4$ in Porous Carbon. A series of ^{7}Li and ^{11}B single pulse excitation spectra were measured for different loadings of $LiBH_4$ melt infiltrated in porous carbon. These spectra are shown in Figure 1. In these series, 25−30 wt % $LiBH_4$ corresponds to complete pore filling. Figure 1c,g shows the ^{7}Li and ^{11}B spectra of a physical mixture containing 25 wt % $LiBH_4$ and 75 wt % nanoporous carbon and the same sample after melt infiltration. The physical mixture (Figure 1g) shows single resonances for ^{7}Li and ^{11}B at −2.7 and −42.9 ppm, respectively, in agreement with previous studies.[59] However, compared to the pure compounds, a small decrease in shift of approximately 1−2 ppm and an increase in line broadening are observed after physically mixing the material with carbon. This line broadening was also observed for $NaAlH_4$ mixed with the same type of porous carbon, HSAG-500. Since graphitic carbon has an unusually large anisotropic magnetic susceptibility, the line broadening is explained by susceptibility effects of the carbon material.

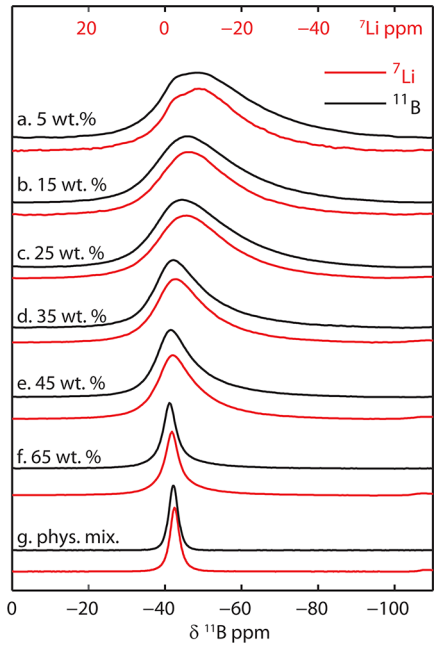

Figure 1. ^{11}B and ^{7}Li single pulse excitation spectra of $LiBH_4$ in porous carbon for different loadings of $LiBH_4$. The lower curves represent the spectra for the physical mixture of the $LiBH_4$ with the porous carbon before melt infiltration. These measurements were done at 14.1 T, and a sample spinning speed of 15 kHz was applied. The ^{7}Li axis (above) is shifted by −40.5 ppm with respect to the ^{11}B axis (below) be able to compare the line shapes with the ^{11}B spectra.

A detailed description of magnetic susceptibility broadening is given by Samoson et al.[60] A magnetic moment will be induced in the sample substance, in our case nanoporous carbon, and generate a local magnetic field at the site of the spin. If the susceptibility is isotropic, the induced magnetic moment is constant and along the magnetic field. In this case, the local field contribution to nuclear spins is similar to a heteronuclear dipolar interaction that will be averaged by magic angle spinning. However, the local field contributions of anisotropic magnetic susceptibility effects are not averaged by magic angle spinning. This causes a shift in peak position and explains the decrease in frequency of the resonances in our

dx.doi.org/10.1021/jp306175b | J. Phys. Chem. C 2012, 116, 22169−22178

spectra. Variations in the location of $LiBH_4$ crystallites with respect to the carbon material are present. This results in a spread of resonance lines and explains the observed line broadening. In general, this line broadening caused by anisotropic susceptibility effects is proportional to the Larmor frequency and therefore remains constant if the spectra are displayed on a parts per million scale.[61]

The ^7Li and ^{11}B resonances strongly broaden after melt infiltration. This effect was observed before in nanoconfined $NaAlH_4$.[38] For a detailed discussion of line broadening mechanisms in nanoconfined complex metal hydrides, we refer to ref 38. In this study, the line broadening in NMR spectra of melt infiltrated $NaAlH_4$ was attributed to susceptibility effects combined with possible distributions in chemical shift values and quadrupolar interaction parameters.

The quadrupolar parameters of bulk $LiBH_4$ are small, for ^{11}B: C_q = 99 kHz and η_q = 0.91 and for ^7Li: C_q = 17.9 kHz and η_q = 0.28−0.98 were found by Arnbjerg et al.[59] Based on these quadrupolar parameters, a second-order line broadening of about 2.4 Hz for ^{11}B and 0.06 Hz for ^7Li is expected at 14.1 T.[62] The experimental line widths of bulk $LiBH_4$ are 400 and 500 Hz, respectively, and therefore the residual line widths cannot be explained by a second-order quadrupolar effect. The ^7Li and ^{11}B bulk $LiBH_4$ resonances are narrow lines when magic angle spinning is applied, indicating that the dipolar couplings are efficiently suppressed. Therefore, it is unlikely that after melt infiltration residual dipolar couplings are the dominating line broadening mechanisms. This observation was indeed confirmed by proton decoupling experiments showing no change in line widths as shown in Figure S1 of the Supporting Information. This means that the line broadening of ^{11}B and ^7Li in nanoconfined $LiBH_4$ in carbon is not dominated by residual dipolar couplings with protons.

To reveal the nature of the NMR line broadening in the nanoconfined $LiBH_4$ samples, we did single pulse excitation measurements and MQMAS experiments for different loadings of $LiBH_4$ in carbon. The single pulse data are shown in Figure 1. It should be noticed that in this figure the maximum intensities are scaled to the same height for each graph. For increasing loadings of $LiBH_4$ in carbon, a continuous decrease in line width for both ^{11}B and ^7Li is observed. For the sample containing 65 wt % $LiBH_4$, about 50% of the $LiBH_4$ is expected to be outside the pores, and thus it can be seen that the spectra become more similar to the physically mixed sample. A table with the line broadening as a function of the $LiBH_4$ loading can be found in Table 1.

Table 1. Observed Fwhm of the Spectra of Figure 1 (in ppm)[a]

sample	^7Li	^{11}B
5 wt % $LiBH_4$	25.8	26.9
15 wt % $LiBH_4$	21.8	24.2
25 wt % $LiBH_4$	21.4	22.5
35 wt % $LiBH_4$	15.3	15.0
45 wt % $LiBH_4$	11.6	10.3
65 wt % $LiBH_4$	5.9	4.2
PM $LiBH_4$	3.0	2.9
$LiBH_4$	2.0	2.0

[a]These spectra were measured at 14.1 T, and a sample spinning speed of 15 kHz was applied.

Remarkably, the ^{11}B and ^7Li line widths are similar when plotted on a ppm scale. This suggests that the dominating mechanism for the line broadening is based on anisotropic susceptibility effects. These anisotropic susceptibility effects result in different magnetic fields for different positions of $LiBH_4$ with respect to the carbon. This results in frequency distributions in the NMR spectra. Because the resonance frequencies are proportional to the magnetic field strength, a region with an altered field strength has all of its resonance frequencies (Li, B) shifted by the same fraction in the ppm scale.[61] We expected that nuclei very close together experience the same magnetic field, and therefore similar line shapes for both ^{11}B and ^7Li are expected. In addition, because ^7Li has a much smaller chemical shift range and smaller typical quadrupole interaction strength than ^{11}B, the equal size of the broadenings for these two nuclear spins indicates that chemical shifts and quadrupole effects are indeed not responsible. The carbon material is highly disordered; hence, it is not possible to calculate the field distribution in the pores, and a quantitative prediction of the spectral shape is presently not feasible. However, the change in line width as a function of loading suggests that the microstructure and/or distribution in the carbon pores depends on the degree of loading.

Only a single component is visible in the spectra, and the line widths change smoothly with increasing loadings. This effect suggests that all $LiBH_4$ in the melt infiltrated nanocomposites is in rather close contact with the carbon in contrast to the physical mixture. No large $LiBH_4$ crystals like in the bulk material are formed, since these would result in a more narrow line shape (as in the physical mixture) superimposed on the broad line. On the basis of the external surface area of the carbon of 10−15 m^2/g, assuming that the pores are completely filled and the remaining $LiBH_4$ is uniformly distributed outside over the porous particles, we estimate that the $LiBH_4$ layer outside the porous particles has a 50−150 nm thickness. So this is indeed far from bulk, but also not in the lower nanometers regime that is found inside the pores.

MQMAS experiments were performed to rule out the possibility of quadrupolar line broadening as the dominant line broadening effect. In this type of experiment, a distribution in field strength would be visible as a chemical shift distribution along the diagonal axis in a MQMAS experiment as has been shown before for $NaAlH_4$.[38] For three different loadings of 5, 25, and 45 wt %, ^{11}B MQMAS spectra were acquired, and these results are shown in Figure 2. All three spectra show a clear broadening along the isotropic shift axis, which confirms that the line broadening is indeed caused by susceptibility effects. The line broadening in the perpendicular direction is symmetric and is attributed to an incomplete removal of residual dipolar couplings.

Possibly the presence of a larger interface area for lower loadings because of incompletely filled pores could result in a higher structural disorder. Structural disorder can be visible as distributions in quadrupolar parameters in the MQMAS experiments. However, no broadening and/or bending in the quadrupolar induced shift direction is visible in these spectra. This means that, within the detection limits, no distributions in quadrupolar coupling parameters can be observed. Therefore, we conclude that the BH_4^- anions are most likely intact. Distortions in these anions like a hydrogen vacancy would have resulted in strong electric field gradients at the position of the nucleus leading to distributions in quadrupolar parameters. In addition, in the case of hydrogen vacancies, we would expect

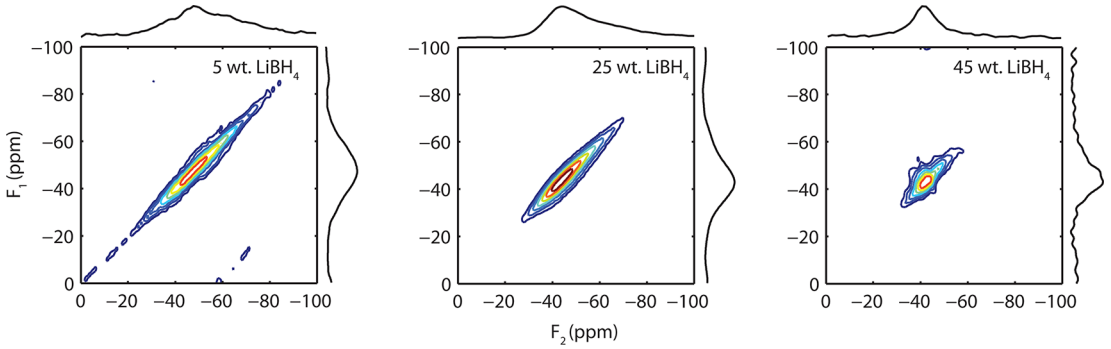

Figure 2. ^{11}B MQMAS spectra of $LiBH_4$/C for different loadings of $LiBH_4$ in porous carbon. These spectra are measured at 14.1 T, and 15 kHz MAS was applied. The spectra are sheared and the vertical axes (F_1) are scaled by a factor of 9/34, so the chemical shift is along the diagonal.

significant differences in chemical shift for ^{11}B, which is not observed.

In a previous study, the anisotropic susceptibility broadening because of the contact to the carbon has been used to study the microstructural evolution of the boron phases in $LiBH_4$ nanocomposites upon dehydrogenation and rehydrogenation.[41] The effect of a catalyst such as nickel on the microstructure of the material was that the $LiBH_4$ distribution in the carbon is retained upon cycling as similar ^{11}B line shapes are observed before and after rehydrogenation. In contrast, different ^{11}B line shapes are observed when no nickel catalyst is present. This result suggests a change in microstructure or distribution of $LiBH_4$ in the carbon material with a tendency toward phase separation and increased cluster size. In this way, the carbon susceptibility can be used to probe the microstructure of the nanoconfined materials. Unfortunately, this effect also comes together with a decrease in resolution and probably structural information will be lost.

$LiBH_4$ in Ordered Mesoporous Silica. To circumvent the large line broadening of $LiBH_4$ nanoconfined in carbon, we continued our study with $LiBH_4$ confined in porous silica. The magnetic susceptibility of silica is much lower than that of graphite. For that reason, we hoped to reduce these susceptibility broadenings that might overshadow structural information. Silica is not an obvious choice to confine $LiBH_4$, as it thermodynamically is expected to react forming lithium silicates. Indeed, it is known that upon decomposition of $LiBH_4$ reaction with the silica takes place, leading to irreversible hydrogen loss.[63] Therefore, this material is not suitable to be used in practical applications. However, it has been proven that sufficiently high hydrogen pressure during melt infiltration can prevent decomposition of the $LiBH_4$ and that under these conditions the porous silica matrix is not damaged by the melt infiltration process.[63] In this work, we study the structural properties of $LiBH_4$ confined in ordered porous silica, MCM-41, with an average pore size of 1.9 nm. It is used as a model system to investigate the fundamental effects of nanoconfinement, which will be equally relevant/applicable for carbon-based systems.

Single Pulse ^{11}B, ^{1}H, and ^{7}Li NMR as a Function of Temperature. ^{11}B, ^{1}H, and ^{7}Li NMR single pulse excitation spectra with and without proton decoupling are measured as a function of temperature for $LiBH_4$ confined in ordered porous silica, MCM-41. This silica has a monodisperse pore size of 1.9 nm. In the ^{11}B spectra at room temperature (Figure 3), a substantially smaller line width is observed in comparison with the spectra in porous carbon. For $LiBH_4$ in MCM-41 measured

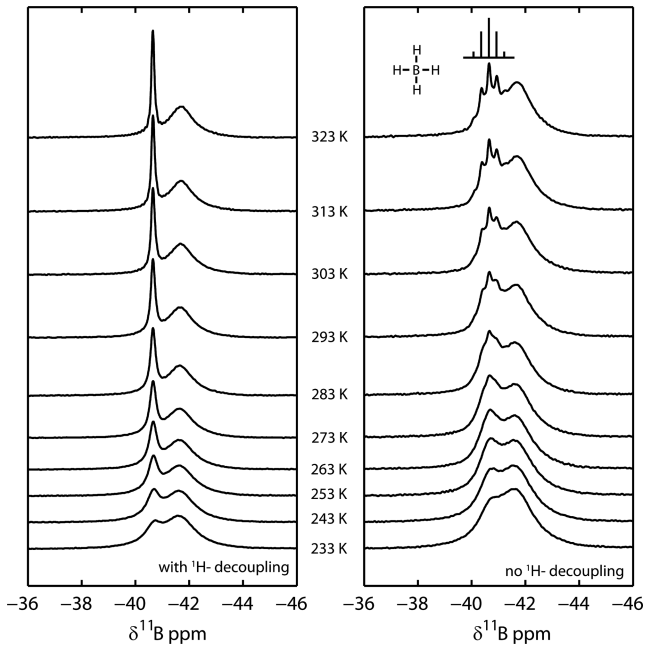

Figure 3. ^{11}B single pulse excitation spectra of 30 wt % $LiBH_4$ in ordered porous silica, MCM-41, for different temperatures with and without ^{1}H decoupling. These measurements were done at 20.0 T, and a sample spinning speed of 17.5 kHz was applied. A clear splitting of the line shape in two components, a broad and a narrow component, is observed when proton decoupling is applied. Above T = 313 K, the spectra without ^{1}H decoupling show a typical J-coupling quintuplet consisting of five lines corresponding to a highly mobile BH_4^- species, where one ^{11}B is coupled to four ^{1}H atoms.

without proton decoupling at 293 K, the approximate fwhm of the line is 2 ppm, while in carbon it was 22.5 ppm. This large decrease in line width is attributed to the absence of the strong susceptibility effects in the MCM-41 material, as expected.

In the ^{11}B single pulse excitation spectrum at 293 K, a clear splitting of the line shape in two components, a broad and a narrow component, is observed when proton decoupling is applied. The broad component is positioned at −41.7 ppm and has a similar shape and position as the bulk $LiBH_4$ material, which was found at −41.5 ppm (see Supporting Information Figure S2) To study the origin of the narrow component in more detail, ^{11}B spectra were measured at different temperatures with and without proton decoupling. A temperature range of T = 233−323 K was chosen. The application of higher temperatures was not possible in this setup. In $LiBH_4$, rotational motion of BH_4^- units has been observed.[2−7] In our

dx.doi.org/10.1021/jp306175b | J. Phys. Chem. C 2012, 116, 22169−22178

spectra, the broad bulk-like component does not differ with temperature. This means there is no change in mobility for BH_4^- in this phase on the approximately milliseconds time scale of our experiments.

Two spectral effects are observed for the narrow component. First, a clear increase in ^{11}B line width is observed upon lowering the temperature. The fact that the line width of the narrow component changes with temperature suggests that there is additional temperature-dependent atomic mobility present. The line broadening in the spectra is most likely caused by residual dipolar couplings, which are not completely removed by magic angle spinning. The atomic motion becomes slower upon lowering the temperature since the lines become broader and dipolar interactions are averaged to a lesser extent. Second, the narrow component shows a splitting in five lines starting at temperatures of 283−293 K and higher when the NMR experiment is done without proton decoupling. The five lines correspond to a typical $^{11}B-^{1}H$ *J*-coupling pattern which, as expected, disappears when proton decoupling is applied. A similar *J*-coupling pattern has been observed by Shane et al.[6] for molten $LiBH_4$ and is attributed to highly mobile BH_4^- species. In this species, a boron atom is coupled to four equivalent hydrogen nuclear spins. This results in a *J*-coupling quintuplet of five lines with intensity ratio 1:4:6:4:1.

The splitting between the ^{11}B lines in our experiment, which equals the *J*-coupling constant, is 80 ± 1 Hz. This value is in agreement with the *J*-coupling constant determined by Shane et al.[6] To prove that we indeed observe a *J*-coupling pattern, a ^{11}B 2D *J*-resolved NMR at 323 K was performed (Figure 4). This

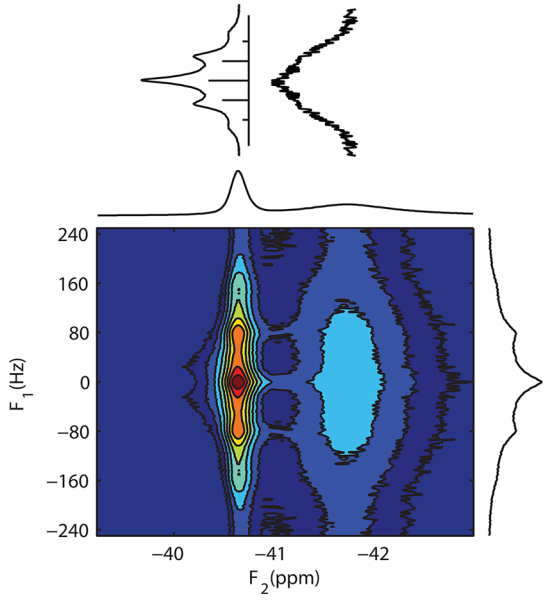

Figure 4. ^{11}B *J*-resolved spectrum of 30 wt % $LiBH_4$ in ordered porous silica, MCM-41, at a temperature of 323 K, measured at 20.0 T using a sample spinning speed of 17.5 kHz. A typical *J*-coupling pattern of one ^{11}B atom coupled to four ^{1}H atoms is observed corresponding to a highly mobile BH_4^- species.

result clearly shows the five-line *J*-coupling quintuplet for the highly mobile compound in the second dimension. The broad component does not show this splitting because it does not experience strong motional averaging.

In the study of Shane et al., the *J*-coupling pattern was observed in liquid $LiBH_4$ by heating the material up to 558 K. Remarkably, for nanoconfined $LiBH_4$, this typical pattern is observed far below the melting temperature of the material and is already observed at 293 K. This means that the mobility of BH_4^- in $LiBH_4$ is strongly increased by nanoconfinement, and its spectrum resembles the spectrum of liquid $LiBH_4$ far below the melting point of bulk $LiBH_4$.

When there is a *J*-coupling pattern visible in the ^{11}B spectra due to the presence to $^{11}B-^{1}H$ *J*-couplings, we may of course expect to observe also a *J*-coupling pattern to be visible in the proton spectra due to $^{1}H-^{10}B/^{11}B$ couplings. Indeed, starting at 303 K, a four-line pattern superimposed on the broad line becomes visible. This pattern can be assigned to mobile BH_4^- species as follows: A proton coupled to a single ^{11}B atom with spin quantum number $I = 3/2$ will result in a splitting in four lines with equal intensity. A proton coupled a single ^{10}B atom with spin quantum number $I = 3$ will result in a splitting in seven lines with equal intensity. These two spectra are shown in Figure 5. The splitting between the lines caused by the $^{1}H-^{10}B$

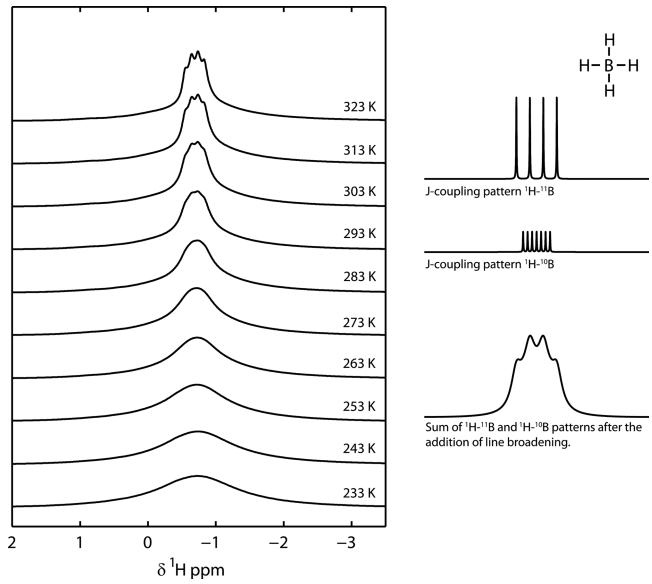

Figure 5. ^{1}H single pulse excitation spectra of 30 wt % $LiBH_4$ in ordered porous silica (MCM-41) for different temperatures observed at 20.0 T and a sample spinning speed of 17.5 kHz was employed. Above $T = 303$ K, the spectra are in agreement with a typical *J*-coupling pattern consisting of the sum of four lines originating from the $^{1}H/^{11}B$ coupling and seven lines corresponding to the $^{1}H/^{10}B$ coupling. This pattern agrees well with the expected pattern of a highly mobile BH_4^- species.

and $^{1}H-^{11}B$ *J*-couplings will be proportional to the ratio of the gyromagnetic constant of ^{10}B and ^{11}B, $\gamma_{^{10}B}/\gamma_{^{11}B}$, which is approximately a factor 3. When these two subspectra are added, while taking a natural abundance into account of 80.1% and 19.9% for ^{11}B and ^{10}B, respectively, the line shape originating from the *J*-coupling pattern in the experimental spectrum is reproduced. The ^{1}H splitting due to the coupling of the ^{11}B nuclear spins equals 80 ± 1 Hz, in agreement with the observed *J*-coupling in the ^{11}B spectra. The resolution of the spectrum is not sufficient to determine the *J*-couplings between ^{1}H and ^{10}B, and these are therefore qualitatively described.

Finally, we show the ^{7}Li spectra of nanoconfined $LiBH_4$ in porous silica under the same conditions under which the ^{1}H and ^{11}B spectra were acquired (Figure 6). Again, these spectra show a narrow and a broad component, which is more

dx.doi.org/10.1021/jp306175b | J. Phys. Chem. C 2012, 116, 22169−22178

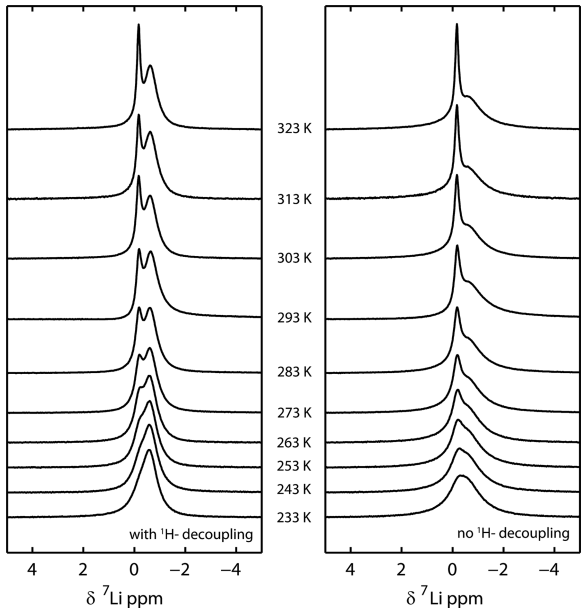

Figure 6. ^{7}Li single pulse excitation spectra of 30 wt % $LiBH_4$ in ordered porous silica (MCM-41) for different temperatures with and without ^{1}H decoupling. These measurements were performed at 20.0 T using a sample spinning speed of 17.5 kHz. These spectra show a narrow and a broad component, which becomes more pronounced when ^{1}H decoupling is applied.

pronounced when ^{1}H decoupling is applied. The narrow component broadens upon lowering the temperature as in the ^{1}H and ^{11}B spectra. No scalar couplings are observed, contrary to the ^{1}H and ^{11}B spectra, since $^{7}Li^{+}$ is not covalently bonded to other nuclei.

In Figure 7, the line widths and relative intensities of the ^{11}B and ^{7}Li resonances for the highly mobile narrow and bulklike broad component are plotted. We attribute the line widths of these spectra to residual dipolar couplings which are not completely averaged by magic angle spinning. The line widths of ^{7}Li and ^{11}B of the broad component do not change with temperature. This means that there is no change in atomic mobility at the approximately milliseconds time scale in this temperature range. The resonances of the narrow component clearly broaden when the temperature is lowered. This means that the mobility of the BH_4^- units is reduced upon lowering the temperature. The relative intensities of the narrow and broad components stay equal when the temperature is varied. This indicates that there is no exchange between two distinctly different fractions in the material. This in contrast to what was observed by Shane et al.[33] As in their study the fraction of motionally narrowed intensity decreased with decreasing temperatures.

Melting of undoped bulk $NaAlH_4$ under excess H_2 pressure to avoid decomposition of the material, resulting in the creation of an additional narrow resonance in the ^{27}Al spectra corresponding to a new highly mobile species.[28] Similar effects might occur in $LiBH_4$. The mobile BH_4^- species could possibly be formed in the bulk material too without the presence of a nanoporous material. To prove that the creation of the highly mobile BH_4^- species is an effect of nanoconfinement and does not take occur in the bulk material, bulk $LiBH_4$ was molten and recrystallized. ^{11}B single pulse excitation spectra of $LiBH_4$ in its pure form and $LiBH_4$, which has been molten and recrystallized, were measured at temperatures of 293 and 323 K. The

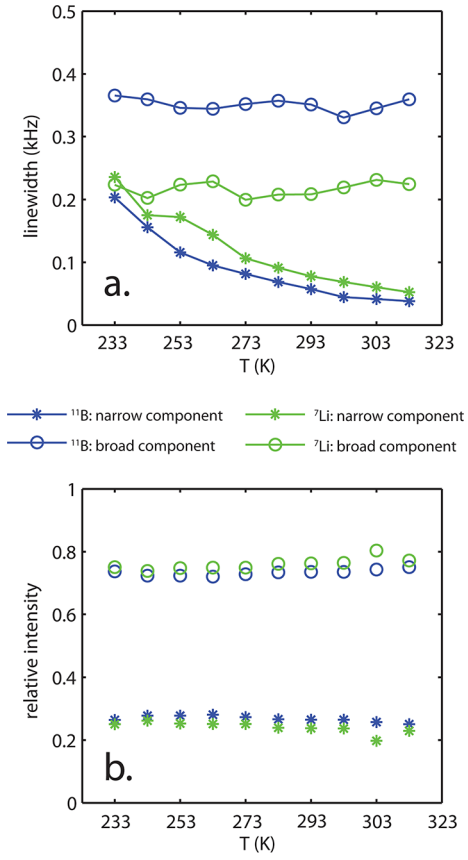

Figure 7. (a) Line widths of the broad and narrow component in the ^{11}B and ^{7}Li single pulse excitation spectra measured with ^{1}H decoupling as shown in Figures 3 and 6. (b) Relative intensities of these two components. These measurements were performed at 20.0 T using a sample spinning speed of 17.5 kHz.

result is shown in the Supporting Information, Figure S2. No narrow components corresponding to highly mobile BH_4^- species were observed in the spectra of $LiBH_4$ which has been molten and recrystallized. This result shows that the enhanced mobility of BH_4^- in the nanoconfined samples is not an effect of the melting procedure alone but originates from the contact with the support material and/or decreased particle sizes.

Static NMR and Second Moment Calculations on $LiBH_4$. The ^{11}B MAS measurements show that there are highly mobile BH_4^- species present in nanoconfined $LiBH_4$ in porous silica. These motions may have both translational and rotational components. To be able to distinguish between these two types of motion, we measured a static spectrum of the material and compared the result with second moment calculations. Our previous study of Na_3AlH_6 showed that this may be a useful method to study different types of motions in complex metal hydrides.[56] A bulk ^{11}B spectrum of $LiBH_4$ was measured, and the result is shown in Figure 8. This spectrum was fitted with a quadrupolar powder pattern, which was simulated using SIMPSON.[64] The following parameters $\eta_q = 0.47 \pm 0.02$, $C_q = 100 \pm 2$ kHz, and a Gaussian line broadening with a fwhm of 7.0 kHz were used. This experimental line broadening was compared with second moment calculations. The expected dipolar broadening of ^{11}B with its surrounding nuclei, ^{11}B, ^{10}B, ^{1}H, ^{6}Li, and ^{7}Li, in the case of a rigid lattice is expected to be 47.2 kHz. This is much broader than the experimental line

dx.doi.org/10.1021/jp306175b | J. Phys. Chem. C 2012, 116, 22169−22178

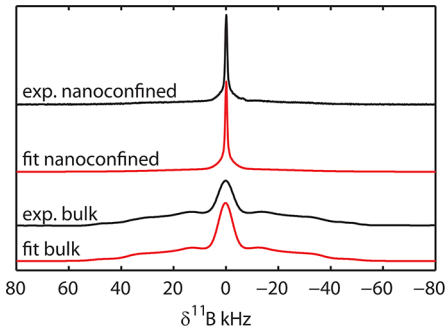

Figure 8. Static ^{11}B spectrum of bulk $LiBH_4$ and 30 wt % $LiBH_4$ confined in porous silica, measured at 20 T, a temperature of 293 K and no magic angle spinning was applied. The bulk spectrum was fitted with an quadrupolar powder pattern with the following parameters: η_q = 0.47 ± 0.02, C_q = 100 ± 2 kHz, and a Gaussian line broadening with a fwhm of 7.0 kHz. The nanoconfined sample was fitted with the same pattern as bulk $LiBH_4$ and one Lorentzian/Gaussian line with a fwhm of 0.9 kHz and a Lorentzian/Gaussian fraction of 0.84.

width. This is explained by the fact that BH_4^- anions experience rotational motions, and this effect is described in various earlier studies.[3−8] Therefore, the second moment calculation is repeated assuming fast isotropically rotating BH_4^- anions. This model of fast isotropically rotating BH_4^- anions is representative for any reorientation mechanism where the four hydrogen atoms move over all four possible positions in the BH_4^- anion. From the perspective of boron, which is situated in the center of the borohydride anions, the dipolar couplings to other boron and lithium nuclei remain unperturbed, since their relative positions should remain fixed. The intraanion interactions between boron and hydrogen in the same anion are fully averaged, and the interanion interactions between different anions are partially averaged. This gives a calculated line width of 7.0 kHz, which is in good agreement with the experimental value. A similar result has been obtained by Jimura et al.[34] where second moments of ^1H and ^{11}B spectra suggest isotropic rotation of BH_4^- above 170 K in the low-temperature phase of $LiBH_4$.

Table 2. Experimental and Calculated Fwhms in kHz of Bulk and Nanoconfined $LiBH_4$[a]

	fwhm (kHz)	^{11}B	^7Li
calculations	rigid lattice $LiBH_4$	47.2	16.7
	contribution of $^{11}B-^{10}B/^{11}B$ interactions to the rigid lattice line width	2.1	X
	isotropically rotating BH_4^- anions, total line width	7.0	11.2
experiment	bulk $LiBH_4$	7.0	11.7
	broad component nanoconfined $LiBH_4$	7.0	11.7
	narrow component nanoconfined $LiBH_4$	0.9	0.9

[a]No magic angle spinning was applied in these measurements.

The same experiment was done for the nanoconfined sample, which is also shown in Figure 8. This spectrum was fitted with two lines. First, a quadrupolar powder pattern as in bulk $LiBH_4$ with η_q = 0.47 ± 0.02, C_q = 100 ± 2 kHz, and a Gaussian line broadening with a fwhm of 7.0 kHz was used. Second, a residual line was fitted without predetermined shape and width, resulting in a width of 0.9 kHz and a Lorentzian/Gaussian fraction of 0.84. An example of such a fit for the spectrum obtained at 293 K is depicted in Figure 8. The first fraction, which gives rise to the 7.0 kHz Gaussian line, is identified as bulklike $LiBH_4$ with rotating borohydride anions. The second fraction, giving rise to a resonance with an line width of 0.9 kHz which is much narrower than 7.0 kHz, must possess additional mobility. This additional mobility is most likely diffusion of the borohydride anions through the material. Rapid translational motion at room temperature of hydrogen, as BH_4^- anions, has been observed by Shane et al. before in nanoconfined $LiBH_4$.[33] Another possible scenario where the boron atoms remain at their positions and hydrogen and lithium translate is not plausible. In this case only the $^{11}B-^{10}B/^{11}B$ interactions remain, resulting in a line width equal to 2.1 kHz, which is larger than the experimental line width of 0.9 kHz. If the diffusion of BH_4^- is sufficiently fast, all dipolar couplings between ^{11}B and its surrounding nuclei should average to zero. However, because there is still a residual line width observed of 0.9 kHz, these translational motions may not be so fast to completely average all dipolar interactions or the BH_4^- anions may prefer to move between a limited amount of positions.

The relative intensities of the narrow component and the quadrupolar powder pattern in the static experiment are shown in Table 3. These values are compared with previously

Table 3. Relative Intensities of the Narrow and Broad Component in Static and MAS NMR Experiments at a Temperature of 293 K

		narrow component	broad component
^{11}B	MAS	0.26	0.74
	static	0.25	0.75
^7Li	MAS	0.24	0.76
	static	0.26	0.74

determined intensities of the MAS spectrum. As expected, the intensities in the static experiment for the two components are in good agreement with the intensities determined in the MAS spectra.

From the MAS data it is not immediately clear if the lithium atoms are mobile as well. Therefore, static measurement and second moment calculations are done for ^7Li, too. The result is shown in Figure 9 together with results on bulk $LiBH_4$. The bulk ^7Li spectrum shows a single broad resonance which is fitted with an Gaussian with a fwhm of 11.7 kHz. No

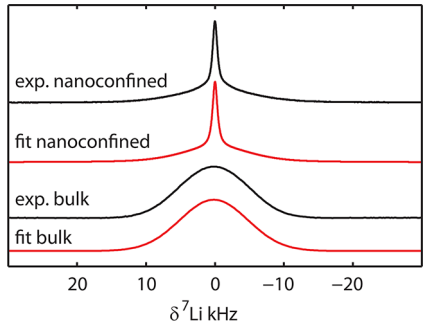

Figure 9. Static ^7Li spectrum of bulk $LiBH_4$ and 30 wt % $LiBH_4$ confined in porous silica, measured at 20 T, a temperature of 292 K and no magic angle spinning was applied. The bulk spectrum was fitted with a Gaussian line broadening with a fwhm of 11.7 kHz. The nanoconfined sample was fitted with a Lorentzian/Gaussian line with a fwhm of 0.9 kHz and a Lorentzian/Gaussian fraction of 0.89.

dx.doi.org/10.1021/jp306175b | J. Phys. Chem. C 2012, 116, 22169−22178

quadrupolar powder pattern is observed because the quadrupolar interaction is relatively small as described before, and the dipolar broadening is the dominating line broadening mechanism. Second moment calculations were done for ^{7}Li assuming fast rotating BH_4^- anions, and this resulted in a line width of 11.2 kHz, which is in agreement with the experimental result of 11.7 kHz. A rigid lattice would have resulted in a line broadening of 16.7 kHz.

The same measurement was performed for the nanoconfined sample. Like in the ^{11}B static spectrum, we see a narrow line superimposed on a broad line. These two fractions are fitted with a Gaussian line broadening with a fwhm of 11.7 kHz and a Lorentzian/Gaussian line with a fwhm of 0.9 kHz and an L/G fraction of 89%. The first fraction, which gives rise to the 11.7 kHz Gaussian line, is again identified as bulklike $LiBH_4$ with rotating borohydride anions. The second fraction corresponds to a different phase, in which the BH_4^- groups experience fast rotational and translational motions. In this case we expect that all dipolar interactions of ^{7}Li with ^{11}B, ^{10}B, and ^{1}H are averaged. The remaining interaction of ^{7}Li with ^{6}Li and ^{7}Li assuming no lithium mobility would result in a line width of 3.4 kHz calculated by second moment calculations. However, our measured line width equals 0.9 kHz, which is much smaller than the calculated line width. Therefore, we can explain this difference by the fact that not only BH_4^- is highly mobile but Li^+, too. The relative intensities of the narrow and broad component are shown in Table 3 and in good agreement with the MAS data.

Static ^{7}Li and ^{11}B measurements of molten $LiBH_4$ by heating the material up to 558 K have been done by Shane et al.[4] Bulk $LiBH_4$ shows a phase transition from an orthorhombic (low temperature) to a hexagonal (high temperature) phase at 384 K.[8] For ^{7}Li, line narrowing takes place immediately upon entering the high temperature phase due to rapid Li diffusion.[4] For ^{11}B this process goes gradually with increasing temperature.[4] Results on nanoconfined $LiBH_4$ by Shane et al.[33] clearly show the solid−solid transition in the ^{7}Li line shapes, with a 10−15 K depression compared to the bulk. Some rapid lithium motion is already present below this transition.

In our results for the nanoconfined material we see a similar line narrowing of ^{7}Li and ^{11}B as in the spectra of bulk $LiBH_4$ in the molten phase measured by Corey et al.[4] However, this strong line narrowing in nanoconfined $LiBH_4$ occurs already at room temperature. So these static measurements confirm our previous conclusion that the mobility of BH_4^- in $LiBH_4$ is strongly increased by nanoconfinement and show that Li^+ becomes highly mobile, too. Because this line narrowing happens already far below the melting point of $LiBH_4$ and also far below the temperature of the bulk phase transition, this could mean that the high temperature phase is stabilized upon nanoconfinement already at room temperature. A more detailed study of the stabilization of the high temperature phase by nanoconfinement is underway.

CONCLUSIONS

The structural properties and atomic mobilities for $LiBH_4$ nanoconfined in porous carbon and silica were studied using ^{1}H, ^{7}Li, and ^{11}B solid-state NMR.

The ^{11}B and ^{7}Li NMR resonances of $LiBH_4$ confined in porous carbon are strongly broadened compared to bulk $LiBH_4$. The line shapes of ^{11}B and ^{7}Li spectra are equal at a ppm scale, and ^{11}B MQMAS spectra show mainly a line broadening in the chemical shift direction along the diagonal. Therefore, we conclude that this line broadening is dominated by distortions in the main magnetic field caused by anisotropic susceptibility effects as a result of a contact of $LiBH_4$ with the nanostructured carbon material. No bulklike spectral features are observed in the nanoconfined material, which means that the $LiBH_4$ material and the carbon are finely dispersed and all $LiBH_4$ is relatively close to carbon.

The susceptibility broadening in the carbon material results in a decrease of resolution in the NMR spectra because the local magnetic field homogeneity decreases. Therefore, structural information which can be derived from the NMR spectra is lost. To circumvent these effects, we studied confined $LiBH_4$ in a porous silica support with a 1.9 nm average pore size. In the ^{7}Li and ^{11}B spectra of $LiBH_4$, besides a bulklike component, an additional more narrow component is observed. Above T = 313 K, the ^{11}B spectra and ^{1}H spectra show typical J-coupling patterns in both ^{11}B and ^{1}H spectra. These patterns originate from highly mobile BH_4^- species in the nanoconfined $LiBH_4$. Upon lowering the temperature, the J-coupling pattern disappears because of reduced mobility. In bulk $LiBH_4$, these highly mobile species with corresponding J-coupling patterns are only observed in the molten phase. This means that nanoconfinement strongly increases atomic anion mobilities of BH_4^- in $LiBH_4$. Additionally, from the line widths of static ^{7}Li and ^{11}B solid-state NMR measurements compared with second moment calculations, we derived that both BH_4^- and Li^+ experience translation freedom for moving through the crystal lattice.

Summarizing, we conclude that nanoconfinement of $LiBH_4$ in porous silica strongly enhances mobility of borohydride anions and lithium. This suggests a stabilization of the high-temperature phase of $LiBH_4$ already at room temperature due to confinement in nanopores. Possibly, for $LiBH_4$ confined in the carbon support, similar effects may occur. However, this will not be directly visible in the spectra because of the line broadenings due to anisotropic susceptibilities.

ASSOCIATED CONTENT

Supporting Information

Figures S1 and S2. This material is available free of charge via the Internet at http://pubs.acs.org.

AUTHOR INFORMATION

Corresponding Author

*E-mail: A.Kentgens@nmr.ru.nl.

Notes

The authors declare no competing financial interest.

ACKNOWLEDGMENTS

Support of NWO for the "Solid State NMR facility for Advanced Materials Science" is gratefully acknowledged. We thank Hans Janssen, Gerrit Janssen, and Jan van Os for technical support. Angeloclaudio Nale and Petra de Jongh acknowledge NWO-ACTS and NWO-Vidi for financial support.

REFERENCES

(1) Schlapbach, L.; Züttel, A. *Nature* **2001**, *414*, 353−358.
(2) Züttel, A.; Wenger, P.; Rentsch, S.; Sudan, P.; Mauron, P.; Emmenegger, C. *J. Power Sources* **2003**, *118*, 1−7.
(3) Hartman, M. R.; Rush, J. J.; Udovic, T. J.; Bowman, R. C., Jr.; Hwang, S. J. *J. Solid State Chem.* **2007**, *180*, 1298−1305.

(4) Corey, R. L.; Shane, D. T.; Bowman, R. C.; Conradi, M. S. *J. Phys. Chem. C* **2008**, *112*, 18706−18710.
(5) Skripov, A. V.; Soloninin, A. V.; Filinchuk, Y.; Chernyshov, D. *J. Phys. Chem. C* **2008**, *112*, 18701−18705.
(6) Shane, D. T.; Bowman, R. C.; Conradi, M. S. *J. Phys. Chem. C* **2009**, *113*, 5039−5042.
(7) Soloninin, A. V.; Skripov, A. V.; Buzlukov, A. L.; Stepanov, A. P. *J. Solid State Chem.* **2009**, *182*, 2357−2361.
(8) Buchter, F.; Lodziana, Z.; Mauron, P.; Remhof, A.; Friedrichs, O.; Borgschulte, A.; Züttel, A.; Sheptyakov, D.; Strässle, T.; Ramirez-Cuesta, A. J. *Phys. Rev. B* **2008**, *78*, 094302.
(9) Matsuo, M.; Nakamori, Y.; Orimo, S.; Maekawa, H.; Takamura, H. *Appl. Phys. Lett.* **2007**, *91*, 224103.
(10) Friedrichs, O.; Remhof, A.; Hwang, S. J.; Züttel, A. *Chem. Mater.* **2010**, *22*, 3265−3268.
(11) Hwang, S. J.; Bowman, R. C.; Reiter, J. W.; Rijssenbeek, J.; Soloveichik, G. L.; Zhao, J. C.; Kabbour, H.; Ahn, C. C. *J. Phys. Chem. C* **2008**, *112*, 3164−3169.
(12) Orimo, S.; Nakamori, Y.; Kitahara, G.; Miwa, K.; Ohba, N.; Towata, S.; Züttel, A. *J. Alloys Compd.* **2005**, *404*, 427−430.
(13) Knacke, O.; Kubaschewski, O.; Hesselmann, K. *Thermochemical Properties of Inorganic Substances*; Springer-Verlag: Berlin, 1991.
(14) Mauron, P.; Buchter, F.; Friedrichs, O.; Remhof, A.; Zwicky, C. N.; Züttel, A. *J. Phys. Chem. B* **2008**, *112*, 906−910.
(15) Gutowska, A.; Li, L. Y.; Shin, Y. S.; Wang, C. M. M.; Li, X. H. S.; Linehan, J. C.; Smith, R. S.; Kay, B. D.; Schmid, B.; Shaw, W.; Gutowski, M.; Autrey, T. *Angew. Chem., Int. Ed.* **2005**, *44*, 3578−3582.
(16) Baldé, C. P.; Hereijgers, B. P. C.; Bitter, J. H.; de Jong, K. P. *Angew. Chem., Int. Ed.* **2006**, *45*, 3501−3503.
(17) Zhang, Y.; Zhang, W. S.; Wang, A. Q.; Sun, L. X.; Fan, M. Q.; Chu, H. L.; Sun, J. C.; Zhang, T. *Int. J. Hydrogen Energy* **2007**, *32*, 3976−3980.
(18) de Jongh, P. E.; Wagemans, R. W. P.; Eggenhuisen, T. M.; Dauvillier, B. S.; Radstake, P. B.; Meeldijk, J. D.; Geus, J. W.; de Jong, K. P. *Chem. Mater.* **2007**, *19*, 6052−6057.
(19) Stephens, R. D.; Gross, A. F.; Van Atta, S. L.; Vajo, J. J.; Pinkerton, F. E. *Nanotechnology* **2009**, *20*, 204018.
(20) de Jongh, P. E.; Adelhelm, P. *ChemSusChem* **2010**, *3*, 1332−1348.
(21) Vajo, J. J. *Curr. Opin. Solid State Mater. Sci.* **2011**, *15*, 52−61.
(22) Gao, J.; Adelhelm, P.; Verkuijlen, M. H. W.; Rongeat, C.; Herrich, M.; van Bentum, P. J. M.; Gutfleisch, O.; Kentgens, A. P. M.; de Jong, K. P.; de Jongh, P. E. *J. Phys. Chem. C* **2010**, *114*, 4675−4682.
(23) Lohstroh, W.; Roth, A.; Hahn, H.; Fichtner, M. *ChemPhysChem* **2010**, *11*, 789−792.
(24) Gross, A. F.; Vajo, J. J.; van Atta, S. L.; Olson, G. L. *J. Phys. Chem. C* **2008**, *112*, 5651−5657.
(25) Bogdanović, B.; Felderhoff, M.; Germann, M.; Hartel, M.; Pommerin, A.; Schuth, F.; Weidenthaler, C.; Zibrowius, B. *J. Alloys Compd.* **2003**, *350*, 246−255.
(26) Verkuijlen, M. H. W.; de Gelder, R.; van Bentum, P. J. M.; Kentgens, A. P. M. *J. Phys. Chem. C* **2011**, *115*, 7002−7011.
(27) Verkuijlen, M. H. W.; van Bentum, P. J. M.; Zabara, O.; Fichtner, M.; Kentgens, A. P. M. *J. Phys. Chem. C* **2011**, *115*, 13100−13106.
(28) Ivancic, T. M.; Hwang, S. J.; Bowman, R. C.; Birkmire, D. S.; Jensen, C. M.; Udovic, T. J.; Conradi, M. S. *J. Phys. Chem. Lett.* **2010**, *1*, 2412−2416.
(29) Babanova, O. A.; Soloninin, A. V.; Skripov, A. V.; Ravnsbaek, D. B.; Jensen, T. R.; Filinchuk, Y. *J. Phys. Chem. C* **2011**, *115*, 10305−10309.
(30) Srinivasan, S.; Magusin, P. C. M. M.; Kalisvaart, W. P.; Notten, P. H. L.; Cuevas, F.; Latroche, M.; van Santen, R. A. *Phys. Rev. B* **2010**, *81*, 10.
(31) Conradi, M. S.; Mendenhall, M. P.; Ivancic, T. M.; Carl, E. A.; Browning, C. D.; Notten, P. H. L.; Kalisvaart, W. P.; Magusin, P. C. M. M.; Bowman, R. C., Jr.; Hwang, S. J.; Adolphi, N. L. *J. Alloys Compd.* **2007**, *446*−*447*, 499−503.
(32) Shane, D. T.; Corey, R. L.; McIntosh, C.; Rayhel, L. H.; Bowman, R. C.; Vajo, J. J.; Gross, A. F.; Conradi, M. S. *J. Phys. Chem. C* **2010**, *114*, 4008−4014.
(33) Shane, D. T.; Corey, R. L.; Rayhel, L. H.; Wellons, M.; Teprovich, J. A.; Zidan, R.; Hwang, S. J.; Bowman, R. C.; Conradi, M. S. *J. Phys. Chem. C* **2010**, *114*, 19862−19866.
(34) Jimura, K.; Hayashi, S. *J. Phys. Chem. C* **2012**, *116*, 4883−4891.
(35) Verdal, N.; Udovic, T. J.; Rush, J. J. *J. Phys. Chem. C* **2012**, *116*, 1614−1618.
(36) Martelli, P.; Remhof, A.; Borgschulte, A.; Ackermann, R.; Strässle, T.; Embs, J. P.; Ernst, M.; Matsuo, M.; Orimo, S. I.; Züttel, A. *J. Phys. Chem. C* **2011**, *115*, 5329−5334.
(37) Bhakta, R. K.; Herberg, J. L.; Jacobs, B.; Highley, A.; Behrens, R.; Ockwig, N. W.; Greathouse, J. A.; Allendorf, M. D. *J. Am. Chem. Soc.* **2009**, *131*, 13198−13199.
(38) Verkuijlen, M. H. W.; Gao, J.; Adelhelm, P.; van Bentum, P. J. M.; de Jongh, P. E.; Kentgens, A. P. M. *J. Phys. Chem. C* **2010**, *114*, 4683−4692.
(39) Shane, D. T.; Rayhel, L. H.; Huang, Z.; Zhao, J. C.; Tang, X.; Stavila, V.; Conradi, M. S. *J. Phys. Chem. C* **2011**, *115*, 3172−3177.
(40) Nielsen, T. K.; Polanski, M.; Zasada, D.; Javadian, P.; Besenbacher, F.; Bystrzycki, J.; Skibsted, J.; Jensen, T. R. *ACS Nano* **2011**, *5*, 4056−4064.
(41) Ngene, P.; Verkuijlen, M. H. W.; Zheng, Q.; Kragten, J.; van Bentum, P. J. M.; Bitter, J. H.; de Jongh, P. E. *Faraday Discuss.* **2011**, *151*, 47−58.
(42) Ngene, P.; van den Berg, R.; Verkuijlen, M. H. W.; de Jong, K. P.; de Jongh, P. E. *Energy Environ. Sci.* **2011**, *4*, 4108−4114.
(43) Cheng, C. F.; Zhou, W. Z.; Park, D. H.; Klinowski, J.; Hargreaves, M.; Gladden, L. F. *J. Chem. Soc., Faraday Trans.* **1997**, *93*, 359−363.
(44) Barrett, E. P.; Joyner, L. G.; Halenda, P. H. *J. Am. Chem. Soc.* **1951**, *73*, 373−380.
(45) Amoureux, J.; Fernandez, C.; Steuernagel, S. *J. Magn. Reson., Ser. A* **1996**, *123*, 116−118.
(46) Medek, A.; Harwood, J. S.; Frydman, L. *J. Am. Chem. Soc.* **1995**, *117*, 12779−12787.
(47) Frydman, L.; Harwood, J. S. *J. Am. Chem. Soc.* **1995**, *117*, 5367−5368.
(48) Man, P. P. *Phys. Rev. B* **1998**, *58*, 2764.
(49) Engelhardt, G.; Kentgens, A. P. M.; Koller, H.; Samoson, A. *Solid State Nucl. Magn. Reson.* **1999**, *15*, 171−180.
(50) Anderson, M. W.; Klinowski, J. *Chem. Phys. Lett.* **1990**, *172*, 275−278.
(51) Van Vleck, J. H. *Phys. Rev.* **1948**, *74*, 1168−1183.
(52) Filinchuk, Y.; Chernyshov, D.; Cerny, R. *J. Phys. Chem. C* **2008**, *112*, 10579−10584.
(53) Goc, R. *Solid State Nucl. Magn. Reson.* **1998**, *13*, 55−61.
(54) Goc, R. *Z. Naturforsch., B: Chem. Sci.* **2002**, *57*, 29−35.
(55) Goc, R.; Zogal, O. J.; Vuorimäki, A. H.; Ylinen, E. E. *Solid State Nucl. Magn. Reson.* **2004**, *25*, 133−137.
(56) Verkuijlen, M. H. W.; van Bentum, P. J. M.; van Eck, E. R. H.; Lohstroh, W.; Fichtner, M.; Kentgens, A. P. M. *J. Phys. Chem. C* **2009**, *113*, 15467−15472.
(57) Mathworks Inc., http://www.mathworks.com.
(58) Abragam, A. *The Principles of Nuclear Magnetism*; Oxford University Press: New York, 1961.
(59) Arnbjerg, L. M.; Ravnsbæck, D. B.; Filinchuk, Y.; Vang, R. T.; Cerenius, Y.; Besenbacher, F.; Jørgensen, J. E.; Jakobsen, H. J.; Jensen, T. R. *Chem. Mater.* **2009**, *21*, 5772−5782.
(60) Samoson, A.; Tuherm, T.; Gan, Z. *Solid State Nucl. Magn. Reson.* **2001**, *20*, 130−136.
(61) Alla, M.; Lippmaa, E. *Chem. Phys. Lett.* **1982**, *87*, 30−33.
(62) Kentgens, A. P. M. *Geoderma* **1997**, *80*, 271−306.
(63) Ngene, P.; Adelhelm, P.; Beale, A. M.; de Jong, K. P.; de Jongh, P. E. *J. Phys. Chem. C* **2010**, *114*, 6163−6168.
(64) Bak, M.; Rasmussen, J. T.; Nielsen, N. C. *J. Magn. Reson.* **2000**, *147*, 296−330.